Veterinary Microbiology 234 (2019) 92–100

Contents lists available at ScienceDirect

Veterinary Microbiology

journal homepage: www.elsevier.com/locate/vetmic

A novel autolysin $AtlA_{SS}$ mediates bacterial cell separation during cell division and contributes to full virulence in *Streptococcus suis*

Yue Zhang[a,b,c,1], Xiaojun Zhong[a,b,c,1], Pengpeng Lu[a,b,c], Yinchu Zhu[a,b,c], Wenyang Dong[a,b,c], Shipra Roy[a,b,c], H.M.A. Hejair[a,b,c], Zihao Pan[a,b,c], Jiale Ma[a,b,c], Huochun Yao[a,b,c,*]

[a] College of Veterinary Medicine, Nanjing Agricultural University, Nanjing 210095, China
[b] OIE Reference Lab for Swine Streptococcosis, Nanjing 210095, China
[c] Key Lab of Animal Bacteriology, Ministry of Agriculture, Nanjing 210095, China

ARTICLE INFO

Keywords:
Streptococcus suis
$AtlA_{SS}$
Autolysin
Cell separation
Virulence

ABSTRACT

Streptococcus suis (SS) is a major pathogen in the swine industry, and also an important zoonotic agent for humans. The novel SS cell surface protein, $AtlA_{SS}$, comprising the special GW module and *N*-acetylmuramidases domain, was designated as a putative autolysin. Indeed, the $atlA_{SS}$ deletion mutant almost completely lost its activity in Triton X-100 induced bacterial autolysis, while the wild-type and C$\Delta atlA_{SS}$ strains showed significant decrease, to less than 20% of the initial OD_{600} values. Unexpectedly, both immunofluorescence and immunogold electron microscopy confirmed that $AtlA_{SS}$ is mainly located in the cell division septum, suggesting autolytic activity in peptidoglycan hydrolysis may be required for cell separation, thus modulating and truncating bacterial chain length. The biofilm capacity of the $AtlA_{SS}$ mutation was reduced ˜ 40%, as compared to the wild-type strain. The $\Delta atlA_{SS}$ strain also attenuated bacterial adherence in human brain microvessel endothelial cells (HBMECs). Furthermore, we confirmed that $AtlA_{SS}$ has fibrinogen/fibronectin binding capacities. In mouse infection model, the $AtlA_{SS}$ inactivation also significantly attenuated bacterial virulence and proliferation in vivo. In conclusion, these results indicate that $AtlA_{SS}$ autolysin modulates bacterial chain length, and contributes to the full virulence of SS during infection.

1. Introduction

Peptidoglycan (PG), the major component in bacterial cell wall, is essential to resist internal osmotic pressure, implement defense function and maintain the cell shape (Scheffers and Pinho, 2005). Bacteria are able to recycle a significant proportion of the PG degradation products during growth and division, which can reduce the release of muropeptides, and thereby escape the host's immune response (Johnson et al., 2013). Tailoring, recycling and remodeling of the PG require specific peptidoglycan hydrolase (PGH) to cleave certain chemical bonds (Vollmer et al., 2008). At present, four common PGH activities have been defined based on the covalent bond cleavage within the PG molecule, and those are four common PGH activities: endopeptidase, *N*-acetylmuramidase, *N*-acetylmuramyl-$_L$-alanine amidase and *N*-acetylglucosaminidase (Layec et al., 2008). Autolysins also belong to the cell wall PGH, and their activity mediates multiple biological functions such as autolysis, cell division and cell wall turnover (Stinemetz et al., 2017). Moreover, certain autolysins have been established as virulence factors among Gram-positive bacteria. The AtlA protein produced by *Streptococcus mutans* has autolytic properties, and contributes to infective endocarditis virulence in the rat models (Jung et al., 2017). In the *Listeria monocytogenes*, p60-deficient mutants showed attenuated invasiveness and virulence (Pilgrim et al., 2003).

Bacterial autolysins have gradually been acknowledged as a potential source of antimicrobial agents, along with bacteriocin and bacteriophage endolysin. Mehta et al. confirmed that AmiBA2446, an autolysin of *Bacillus anthracis* origin, exhibited bacteriolytic activity against *B. anthracis* and *B. cereus* strains (Mehta et al., 2013). Pneumococcal LytA autolysin could significantly reduce peritoneal bacterial counts, as it has therapeutic effects on infection caused by β-lactam-resistant *Streptococcus pneumonia* (Rodriguez-Cerrato et al., 2007). Autolysins are also considered as potential drug targets. Atilano et al. found that Atl autolysin could conceal the PG molecular signature from peptidoglycan recognition proteins (PGRPs) by trimming the peptidoglycan terminal exposed on the cell wall surface, thus helping *Staphylococcus aureus* escape from the *Drosophila* natural immune system

* Corresponding author at: College of Veterinary Medicine, Nanjing Agricultural University, Nanjing 210095, China.
E-mail address: yaohch@njau.edu.cn (H. Yao).
[1] These authors contributed equally to this work.

https://doi.org/10.1016/j.vetmic.2019.05.020
Received 17 February 2019; Accepted 23 May 2019
0378-1135/

(Atilano et al., 2014). LytA has also been shown to help *Streptococcus pneumonia* avoid detection by the innate immune system (Atilano et al., 2014; Bonnet et al., 2017). This novel method that targets and inhibits autolysin activity may therefore reduce bacterial virulence, and enhance the host immune system.

Streptococcus suis (SS) is a Gram-positive, facultative anaerobic bacterial pathogen, which could cause severe economic losses in the swine industry globally (Goyette-Desjardins et al., 2014). In addition, SS is also considered to be an important zoonotic bacterium, which is frequently reported in human cases. In China, two large-scale outbreaks of SS in humans occurred in 1998 and 2005, and caused 52 deaths in total (Tang et al., 2006). Herein, 33 reference serotypes and 27 novel cps loci (Chz and NCL1-26) SS strains have been identified, according to the capsular polysaccharides (Huang et al., 2019; Zhang et al., 2018). Nevertheless, the pathogenic mechanisms of SS remain limited or fragmentary. In our early research, an autolysin protein designated as Atl, containing *N*-acetylmuramyl-$_L$-alanine amidase domain, was reported to be required for full virulence in SS strains (Ju et al., 2012). In this study, we identified and characterized a novel autolysin protein, $AtlA_{SS}$, with the special GW module and *N*-acetylmuramidases domains. Further work demonstrated that $AtlA_{SS}$ plays a key role in the bacterial cell division, thus modulating the chain length of SS CZ130302 strain to the optimal level. Moreover, $AtlA_{SS}$ facilitates biofilm formation and bacterial adherence, and contributes to the pathogenicity of SS. These findings provide valuable insights into the SS pathogenicity, and may promote the development of new treatment strategies for SS induced infections in the future.

2. Materials and methods

2.1. Ethics statement

Six-week-old female specific pathogen free (SPF) BALB/c mice were purchased from Yangzhou University (Comparative Medicine Center). The Department of Science and Technology of Jiangsu Province approved all animal experiments [License number: SYXK (SU) 2017-0007].

2.2. Bacterial strains and culture conditions

The CZ130302, Δ$atlA_{SS}$, CΔ$atlA_{SS}$ and recombinant *E. coli*-pCold II-$AtlA_{SS}$ strains were used in this study (Table 1). All the SS strains were cultured in Todd-Hewitt broth (THB; Becton-Dickinson) containing 3% fetal bovine serum, or solid medium containing 5% (v/v) sheep blood, at 37 °C in 5% CO_2 atmosphere. In order to select mutants, 100 μg/ml spectinomycin (Spc; Sigma) or 10% (w/v) sucrose was added to the medium for screening. In addition, the A medium (2.0% peptone, 1.0% glucose, 0.5% NaCl, 0.393% $K_2HPO_4 \cdot 3H_2O$, 0.01% $MgSO_4 \cdot 7H_2O$, 0.077% KH_2PO_4, 0.002% $MnSO_4 \cdot H_2O$) was used for biofilm formation assay. The *E. coli* strains were grown in Luria-Bertani (LB; Becton) medium. If necessary, 50 μg/ml ampicillin (Amp; Sigma) was added to the LB medium.

2.3. Construction of Δ$atlA_{SS}$ and CΔ$atlA_{SS}$ mutants

To investigate the contribution of $atlA_{SS}$ gene, the Δ$atlA_{SS}$ and CΔ$atlA_{SS}$ strains were achieved using the novel natural DNA transformation in SS (Zhang et al., 2018; Zhu et al., 2019). This study used the $ComS_{13-21}$ peptide (GNWGKWTDG) to stimulate the natural transformation competence of SS. Here, the Δ$atlA_{SS}$ mutant was constructed through 2 steps of natural transformation. First, the up/downstream homologous fragments were amplified by PCR with primers $atlA_{SS}$-L1/$atlA_{SS}$-L2 and $atlA_{SS}$-R1/$atlA_{SS}$-R2 respectively, from the CZ130302 genomic DNA. The *spc* gene was amplified by primers *spc*-1 and *spc*-2 for resistance selection, and *sacB* gene by *sacB*-1 and *sacB*-2 for negative selection (Zhu et al., 2019). The four amplification products above were then ligated by fusion PCR with primers $atlA_{SS}$-L1/$atlA_{SS}$-R2. $ComS_{13-21}$ peptide (250 μM) and fusion fragment (1.2 μg) were added to 100 μl CZ130302 (OD_{600} = 0.035-0.058). The mixture was statically cultured for 2 h at 37 °C, and then applied to the Spc THB-agar medium. Where after, the fusion homologous fragment, without any marker and amplified by primers $atlA_{SS}$-LU/$atlA_{SS}$-LD and $atlA_{SS}$-RU/$atlA_{SS}$-RD, was transferred to the proto-positive mutant for a second transformation. The Δ$atlA_{SS}$ mutant was screened on the THB-agar medium containing 10% (w/v) sucrose. In our study, the CΔ$atlA_{SS}$ strain was also obtained by the above method. All primers used in this study were listed in Table 1.

2.4. Autolysis assays

The autolysis test was performed following an established method (Ju et al., 2012). The CZ130302, Δ$atlA_{SS}$ and CΔ$atlA_{SS}$ strains were grown to an OD_{600} of 0.8, and then washed twice with phosphate-buffered saline (PBS, pH 7.0). The harvested cells were adjusted to an OD_{600} of 0.6 in potassium phosphate buffer (50 mM; pH 7.0) containing 0.05% Triton X-100. The bacterial suspensions cultured at 37 °C were gently shaken, and OD values monitored every hour.

2.5. Indirect immunofluorescence analysis

An immunofluorescence microscopy assay was performed in order to visualize the localization of $AtlA_{SS}$ at the SS surface. Briefly, the CZ130302 and Δ$atlA_{SS}$ strains were grown to exponential phase, and then washed three times with sterile PBS. The 5-μl samples were adsorbed on the cover glasses, and fixed in 4% paraformaldehyde-PBS. After fixation, the samples were blocked with 5% bovine serum albumin (BSA), and then labeled for 2 h at 37 °C with the anti-$AtlA_{SS}$ rabbit polyclonal antibody, at a dilution of 1:250. After thorough washing, the samples were stained with the secondary antibody goat anti-rabbit IgG (H + L), Alexa Fluor 488 (Thermo), diluted at 1:2000. In addition, bacterial DNA was stained by 4′,6-diamidino-2-phenylindole (DAPI; KeyGEN BioTECH). The treated samples were finally visualized on the laser scanning confocal microscopes (Nikon Instruments, Inc. Leica Sp5 AOBS confocal system).

Furthermore, the $AtlA_{SS}$ protein was also tested for binding to human brain microvessel endothelial cells (HBMECs) using the indirect immunofluorescence assays. In short, HBMECs were incubated with 100 μg/ml purified $AtlA_{SS}$ protein for 1.5 h at 37 °C. Moreover, incubation with the recombination HP07325 protein or BSA, which have no cell adhesion properties, was set as the negative group (Li et al., 2017). Treated cells were immobilized with the cold methanol for 30 min, and then incubated with His tag monoclonal antibody (Thermo Fisher) for 2 h at 37 °C, without shaking. The samples without the His tag monoclonal antibody were set as the blank control. Finally, the $AtlA_{SS}$ protein was detected with goat anti-mouse IgG-FITC, and the intracellular nucleoid was stained with DAPI. The processed samples were visualized with the Carl Zeiss LSM710.

2.6. Immunogold electron microscopy

Subcellular localization of $AtlA_{SS}$, was observed through immunogold electron microscopy, as described elsewhere (Zhang et al., 2018). The CZ130302 cells were harvested by centrifugation, and incubated with anti-$AtlA_{SS}$ rabbit antibody at a dilution of 1:100 for 2 h at 37 °C. Additionally, a blank-control group was incubated with pre-immune negative serum. The samples were then labeled with goat anti-rabbit secondary antibody, 10-nm gold-conjugated (Boster, China), diluted at 1:200. The processed bacteria were immobilized for 12 h in 0.1 M sodium chloride buffer containing 2% paraformaldehyde and 2% glutaraldehyde. Finally, the subcellular localization of $AtlA_{SS}$ was observed with the Hitachi-7650 transmission electron microscope (Hitachi Ltd., Japan).

Table 1
Bacterial strains, plasmids, and primers used in this study.

Strain, plasmid, or primer	Description[a] or sequences (5′–3′)[b]	Sources, references or function
Bacterial strains		
CZ130302	A novel variant serotype Chz of SS which caused acute meningitis in piglets	Collected in our lab
P1/7	virulent strain of the SS2	Collected in our lab
HA9801	virulent strain of the SS2	Collected in our lab
ZY05719	virulent strain of the SS2	Collected in our lab
SC070731	virulent strain of the SS2	Collected in our lab
HN105	virulent strain of the SS5	Collected in our lab
GZ0565	virulent strain of the SS9	Collected in our lab
Δ*atlA*$_{SS}$	Deletion mutant of *atlA*$_{SS}$ with CZ130302 background	This study
CΔ*atlA*$_{SS}$	Complemented strain of *atlA*$_{SS}$ with Δ*atlA*$_{SS}$ background	This study
DH5α	Cloning host for maintaining the recombinant plasmids	Invitrogen
BL21(DE3)	Host for expressing the recombinant proteins	Invitrogen
plasmids		
pCold II	His-tag expressing vector, Amp^r	Invitrogen
pCold II-AtlA$_{SS}$	pCold II inserted in-frame with the *atlA*$_{SS}$ gene for expressing AtlA$_{SS}$, Amp^r	This study
Primers		
atlA$_{SS}$-L1	GGAAGTTGAAGCAGCTGCTAG	Upstream of the fusion fragment
atlA$_{SS}$-L2	GTTTTCAGCATTATCCTTTGATTGGTTTCGGTAGTGT	for Δ*atlA*$_{SS}$ (Step 1)
sacB-1	GGATAATGCTGAAAACTCCTTG	Negative selection marker
sacB-2	CACGAACACTAGTTTATTTGTTAACTGTTAATTGTCC	(Step 1)
spc-1	ACTAGTGTTCGTGAATACATGTTA	Spectinomycin resistance gene
spc-2	AATCTGATTACCAATTAGAATG	(Step 1)
atlA$_{SS}$-R1	ATTGGTAATCAGATTCACAAGCAATGTCCATGTCTC	Downstream of the fusion fragment for Δ*atlA*$_{SS}$ (Step 1)
atlA$_{SS}$-R2	GCATCAATCGTGACAACACTC	
atlA$_{SS}$-LU	CTATGTCAACAAAGGCGAAC	Upstream of the fusion fragment
atlA$_{SS}$-LD	GGAATAACCCTACATGTATTTGCTTCTCATTCG	for Δ*atlA*$_{SS}$ (Step 2)
atlA$_{SS}$-RU	GCAAATACATGTAGGGTTATTCCAGATTATA	Downstream of the fusion fragment for Δ*atlA*$_{SS}$ (Step 2)
atlA$_{SS}$-RD	TCACCTCAATCTGACTGCGT	
C-*atlA*$_{SS}$-L1	GCCGTGTTGGAGATGCTGAGT	Upstream of the fusion fragment
C-*atlA*$_{SS}$-L2	GTTTTCAGCATTATCCTAGCCAAAAACAAGCTCACTC	for CΔ*atlA*$_{SS}$ (Step 1)
C-*atlA*$_{SS}$-R1	ATTGGTAATCAGATTAGAATGACCAACATGCTTTCA	Downstream of the fusion fragment for CΔ*atlA*$_{SS}$ (Step 1)
C-*atlA*$_{SS}$-R2	TCAGGGAAGGATGCGTAGGGT	
C-*atlA*$_{SS}$-LU	TACAGTTGGATTTGGGGTCTT	Upstream of the fusion fragment
C-*atlA*$_{SS}$-LD	AACTCCAAATATATCTAGCCAAAAACAAGCTCACTC	for CΔ*atlA*$_{SS}$ (Step 2)
C-*atlA*$_{SS}$	GATATATTTGGAGTTTCACT	The full-length *atlA*$_{SS}$ ORF for CΔ*atlA*$_{SS}$ (Step 2)
C-*atlA*$_{SS}$	AGCTCCACTAGTTCCGATAAT	
C-*atlA*$_{SS}$-RU	GGAACTAGTGGAGCTCCTGCGGTCTAGTTTAGAAT	Downstream of the fusion fragment for CΔ*atlA*$_{SS}$ (Step 2)
C-*atlA*$_{SS}$-RD	AGGGTTGGTCAAAATAAATGG	
AtlA$_{SS}$-L	CgagctcAACACTACCGAAACCAATCAA	Primers for construction of the
AtlA$_{SS}$-D	CCctcgagCTACTTAGTAAATCGATTTGT	pCold II-AtlA$_{SS}$

[a] Amp^r, Ampicillin resistance.
[b] Underlined nucleotides denote reverse complement; Lowercase nucleotides denote restriction enzyme sites.

Table 2
Evaluation of the pathogenicity of SS strains with a mouse infection model.

Dose of challenge (Intraperitoneal injection)	Number of death/total						
	CZ130302	P1/7	HA9801	ZY05719	SC070731	HN105	GZ0565
5×10^6 (CFU/mouse)	7/10	0/10	0/10	0/10	0/10	1/10	0/10

2.7. In vivo challenges of BALB/c mice

Animal experiments were conducted to detect the contribution of *atlA*$_{SS}$ gene to SS virulence. The CZ130302, Δ*atlA*$_{SS}$ and CΔ*atlA*$_{SS}$ strains were grown to exponential phase, and washed three times with PBS. In the survival curves assay, groups of 10 mice were injected intraperitoneally with 3×10^7 CFU/mouse of each SS strain, and the clinical symptoms and death of mice were monitored approximately every 8 h for 14 days. In the LD_{50} assay, the SS strains were adjusted to 5×10^5 - 5×10^8 CFU/ml, with serial ten-fold dilutions. Then, BALB/c mice were randomly divided into 3 groups, with 40 mice in each group, and cohorts of 10 mice were intraperitoneally injected with 200 μl bacterial suspension. The LD_{50} result was calculated by the Reed-Muench method.

Moreover, the bacterial dissemination assay was performed to further evaluate the proliferation and invasion capacity of WT, Δ*atlA*$_{SS}$ and CΔ*atlA*$_{SS}$. Three groups each of 6 BALB/c mice were infected, by intraperitoneal injection, with 1.5×10^7 CFU/mouse of each SS strain. The infected mice were anesthetized by isoflurane, and euthanized with CO_2 at 12 h postinfection. The brains, lungs and kidneys were then collected for weighing and homogenization. Bacteria were identified from blood and organ samples, by plating serial dilutions on the THB agar plates.

2.8. Biofilm assay

Logarithmic phase cultures of WT, Δ*atlA*$_{SS}$ and CΔ*atlA*$_{SS}$ strains were diluted 100 times with A medium, and 200 μl suspension solution was inoculated in 96-well polystyrene plates. To test the stimulation of calcium ions to AtlA$_{SS}$, A medium was supplemented with different concentrations of $CaCl_2$ (50 μM; 100 μM; 250 μM). After 72 h incubation, the free-floating bacteria and liquid medium were discarded, and

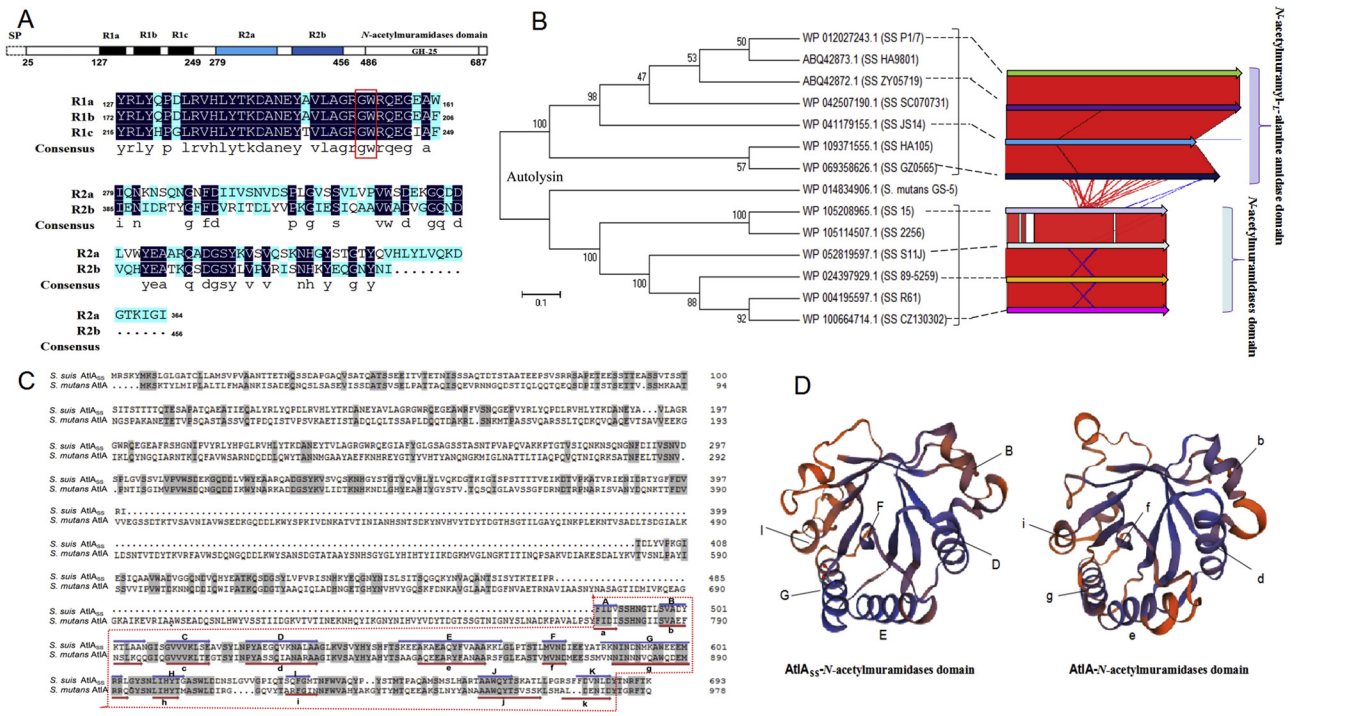

Fig. 1. A novel autolysin protein AtlA$_{SS}$ was identified in *Streptococcus suis*. (A) Schematic representation of AtlA$_{SS}$. The AtlA$_{SS}$ protein contains four main parts: a signal peptide at its N-terminus, a cell wall-anchoring domain (GW) containing three tandem repeats (R1a, R1b, R1c) and a group B Streptococcus Bsp-like peptidoglycan- binding domain (PBD) containing two tandem repeats (R2a, R2b) in the middle, as well as a *N*-acetylmuramidases domain. Dark shade and light shade indicate identical and similar residues, respectively. (B) Phylogenetic relationships of autolysin proteins from streptococcal species. The neighbor-joining tree (bootstrap n = 500) was constructed based on a ClustalW alignment of the autolysin proteins. The visual representation of the alignments of the autolysin genes were determined by the Artemis comparison tool (ACT). (C) Sequence alignments of the autolysin proteins from *S. mutans* GS5 and SS CZ130302. Gray boxes represent the identical residues; red boxes represent the *N*-acetylmuramidases domain; secondary structural elements are shown in the sequences by arrows. (D) The putative structures of the *N*-acetylmuramidases domain in AtlA$_{SS}$ and AtlA proteins. The prediction diagrams were established by the software of SWISS-MODEL, and the secondary structure were also indicated at the corresponding position (For interpretation of the references to colour in this figure legend, the reader is referred to the web version of this article).

the wells washed three times with PBS. The plates were stained with 0.04% crystal violet for 20 min, washed thrice with PBS, and then air dried for 1 h. Crystal violet was extracted by 200 µl 95% (v/v) ethanol, and biofilms quantified by measuring the optical density at 595 nm with the microplate reader (Biotek Instruments Inc). Each assay was performed in triplicate, and wells with bacteria-free A medium served as blank controls.

Additionally, SS strains were cultured on cover glasses placed in 12 well plates for confocal microscopic observations. Following 72 h incubation, the glass slides were gently washed three times with PBS to remove free-floating bacteria, and then stained with Syto 9 green fluorescent dye (Thermo Fisher), according to the manufacturer's instructions. Finally, the three-dimensional structures of SS biofilms were visualized on a Nikon A1 plus si STROM laser scanning confocal microscope.

2.9. Adhesion assays with HBMEC cells

Adhesion assays were performed as previously reported, with some modifications (Zhang et al., 2018). Briefly, HBMEC cells were cultured to monolayer, about 5×10^5 cells/well. The strains in logarithmic phase were washed 3 times with PBS, and incubated with HBMEC cells for 2 h at a bacterium-to-cell ratio of 20:1. The HBMECs were washed 5 times with PBS, and then lysed with 900 µl sterile water and 100 µl trypsin (0.25%). Serial dilutions of the cell lysate were plated onto THB agar plates, and incubated overnight at 37 °C. The adhesion rate of CZ130302 strain was set to 100%. All experiments were repeated three times.

2.10. Assay for binding of SS to fibrinogen and fibronectin

The agar overlay assay evaluated SS strains binding capacity to fibrinogen (FG) and fibronectin (FN). The 6-well tissue culture plates were coated with 2 ml of 100 µg/ml FG or FN for 12 h at 4 °C. The WT, Δ*atlA*$_{SS}$ and CΔ*atlA*$_{SS}$ strains were grown to exponential phase, washed thrice with PBS, and adjusted to a final concentration of about 10^4 CFU/ml. The treated bacterial suspension was inoculated in the substrate-coated wells, with 1.5 ml/well, and then incubated standing at 4 °C for 2 h. The wells were washed 5 times with PBS to remove non-adherent bacteria, and covered THB medium containing 0.75% agar (2 ml/well) with overnight culture. The colony number in each well was measured, and the binding capacity of WT strain was set as 100%. All assays were performed at least three times.

2.11. Recombinant protein binding assays by far-western blot

The binding studies were carried out to validate whether recombinant AtlA$_{SS}$ can specifically bind to the FG and FN. For this purpose, the AtlA$_{SS}$ protein was separated by SDS-PAGE, and then transferred to PVDF membranes (0.22 µm; Millipore). The membranes were blocked with 5% (w/v) skim milk in Tris-buffered saline Tween (TBST) at 37 °C for 2 h, and then incubated with 10 µg/ml FG or FN at 37 °C. Un-incubated protein membranes were set as the blank-control group. Following 2 h incubation, the membranes were washed 3 times with TBST, and incubated with goat anti-human FG antibody (Sigma) and rabbit anti-human FN antibody (Boster) respectively, at a dilution of 1:5000 for 2 h at 37 °C. Subsequently, the processed membranes were stained with the HRP conjugated secondary antibodies (Boster).

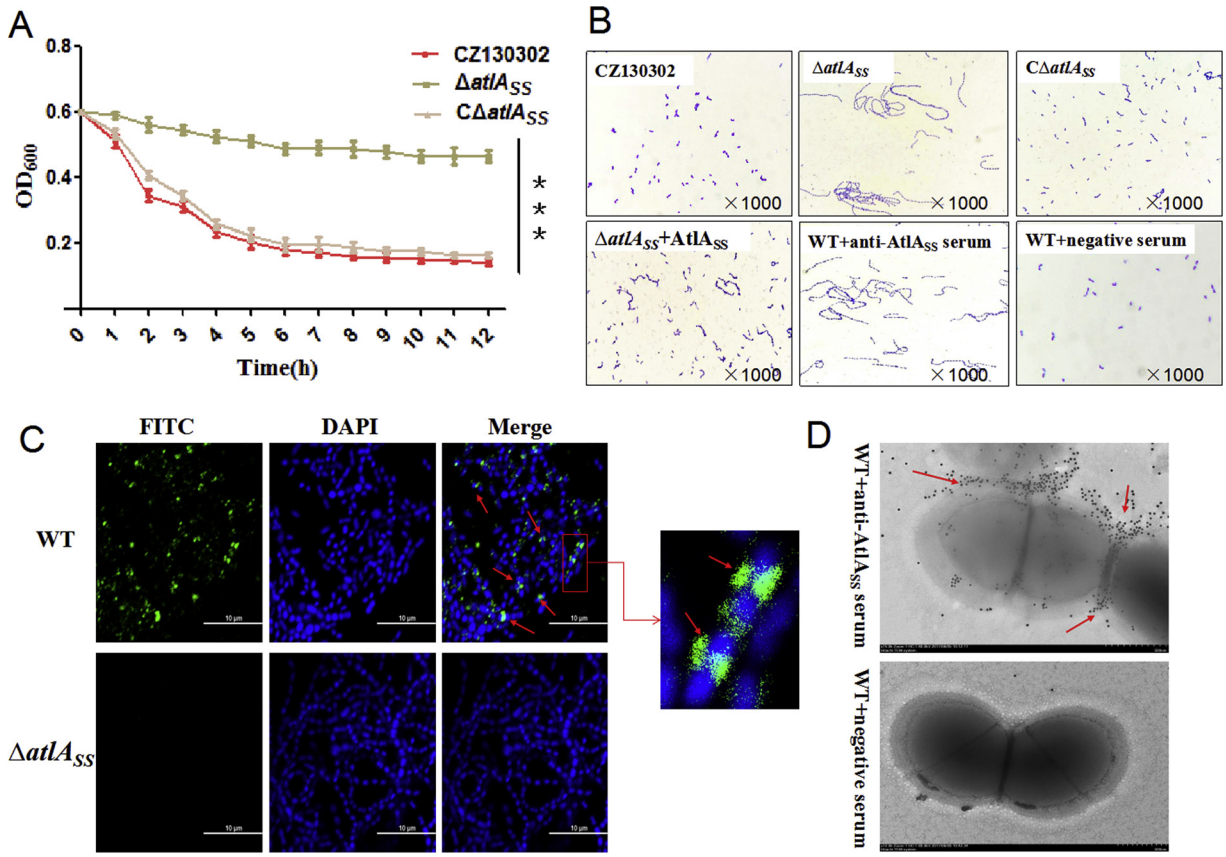

Fig. 2. $AtlA_{SS}$ involved in the cell autolysis and separation. (A) Autolytic activity of the WT, Δ*atlA*$_{SS}$ and CΔ*atlA*$_{SS}$ strains. Cells lytic activity was monitored at OD_{600}. Data are indicated as the means ± SEM from three independent assays (*** $P < 0.001$). (B) Microscopic morphology of WT, Δ*atlA*$_{SS}$, CΔ*atlA*$_{SS}$ and anti-AtlAss antibody treated bacterial cells. Logarithmic phase bacteria were treated with Gram's method and microscopy, and the strains were imaged under the same magnification scale. (C) Localization of $AtlA_{SS}$ on the surface of CZ130302 detected by indirect immunofluorescence assay. The intracellular nucleoid was stained with DAPI in blue and the $AtlA_{SS}$ protein was detected with Alexa Fluor 488 conjugated the goat anti-rabbit IgG (H + L) in green. Red arrows mark the rallying point of $AtlA_{SS}$ protein. White bars represent 10 μm. (D) Immunogold electron micrographs of the SS strain. Bacteria were treated with anti-$AtlA_{SS}$ serum or negative serum. Red arrows point to the immunogold labeling of $AtlA_{SS}$ protein. White bars represent 500 nm (For interpretation of the references to colour in this figure legend, the reader is referred to the web version of this article).

2.12. Statistical analyses

All experiments were performed at least 3 times. The Prism 5 software package was used for statistical analyses. The unpaired two-tailed Student's *t* test and the Log-rank (Mantel-Cox) test were used to analyze the data. For all tests, a P value < 0.05 was considered statistically significant.

3. Results

3.1. SS strain CZ130302 showed significantly shorter bacterial chain length but higher virulence in mouse infection model

CZ130302, as the representative strain of serotype Chz of SS, was isolated from an outbreak of meningitis with a high mortality rate in piglets (Pan et al., 2015; Zhang et al., 2018). Microscopic observation showed that the bacterial chains of CZ130302 strain only consist of three cells on an average, and are significantly shorter than those of other SS strains (Supplemental Fig. 1). Furthermore, CZ130302 strain showed supervirulence in the mouse infection model. As shown in Table 2, the mice group challenged with strain CZ130302 (7/10) had a significantly higher mortality rate than those with other SS virulent strains (P1/7, HA9801, ZY05719, SC070731, HN105 and GZ0565), under the same infective dose and injection method. Therefore, further work to explore the underlying mechanism that modulates bacterial chain length in CZ130302 strain may contribute to a better understanding on its high pathogenicity in the mouse infection model.

3.2. Screening a putative PGH as a potential factor to modulate chain length in CZ130302 strain

It is known that PGH is involved in cell wall turnover, growth and expansion, and also contributes to daughter cell separation during division (Ju et al., 2012; Vollmer et al., 2008). We carried out a whole-genome sequencing for the CZ130302 strain (accession numbers: CP024974.1). Through sequence similarity analysis with other PGHs in streptococci bacteria, we identified a putative PGH in CZ130302 strain, named $AtlA_{SS}$, which may relate to the modulation of bacterial chain length. $AtlA_{SS}$ has 693 amino acids, and a predicted molecular mass of 76 kDa. As shown in Fig. 1A, four main parts were detected in the $AtlA_{SS}$ protein. In addition to an N-terminal putative signal peptide, the protein has a special cell wall-anchoring domain (GW module) containing three tandem repeats (R1a, R1b, R1c) with high similarities in sequence alignment (amino acid identity ranging from 85.7% to 97.1%). Moreover, two repeated sequences R2a and R2b shared 41% identity with each other, and constituted the group B Streptococcus Bsp-like peptidoglycan-binding domain.

It should be noted that the $AtlA_{SS}$ protein was predicted to encode an *N*-acetylmuramidases (GH25 muramidase) domain in its C-terminus. In fact, the putative and identified PG-degrading enzymes from SS could be divided into two deep clades in the phylogenetic tree (Fig. 1B). The $AtlA_{SS}$ protein and AtlA from *Streptococcus mutans* belong to the same

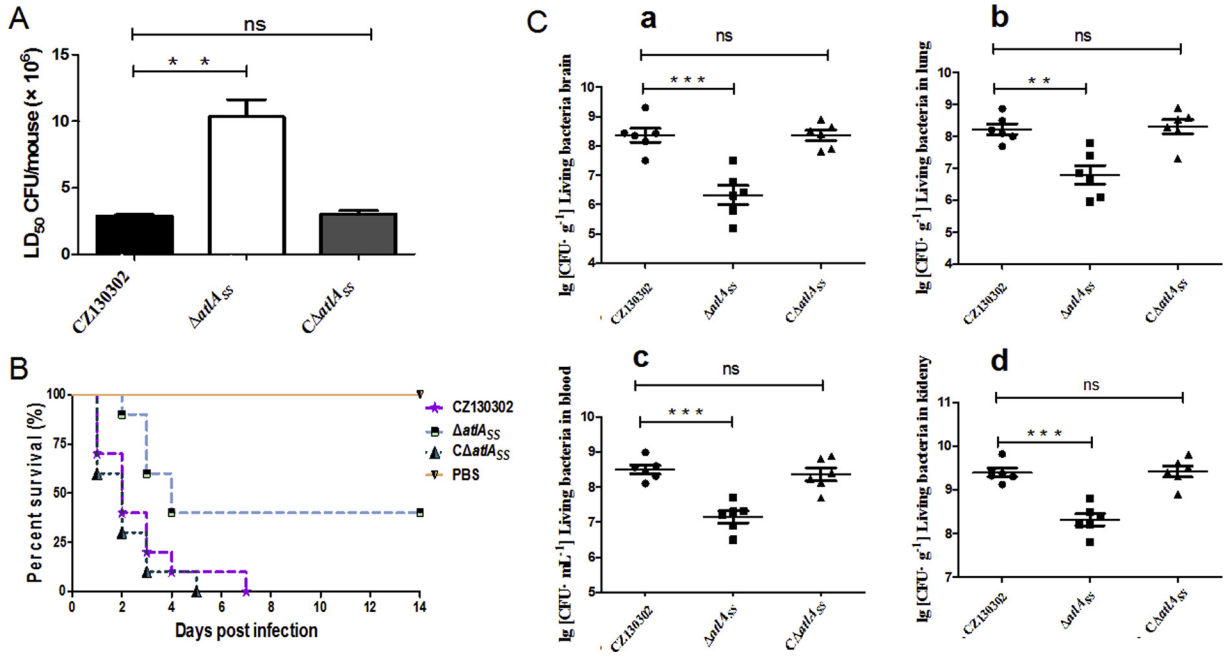

Fig. 3. Effects of *atlA*$_{SS}$ gene on the pathogenicity of SS in mouse infection model. (A, B) LD_{50} evaluation and survival curve of CZ130302, Δ*atlA*$_{SS}$ and CΔ*atlA*$_{SS}$ in the mouse infection model. The six-weeks-old BALB/c mice were infected with indicated SS strains at the same dose and monitored over a 14-day period. Asterisks indicate significant differences in virulence comparing with the wild type strain (** $P < 0.01$). (C) Survival of the CZ130302 and mutant strains in the mice organs. The mice infected with indicated SS strains were sacrificed and examined for bacterial loads in brain (a), lung (b), blood (c), and kidney (d) tissues at 12 h postinfection. Asterisks indicate significant differences (** $P < 0.01$; *** $P < 0.001$).

branch, and the latter has been identified as the functional autolysin in *N*-acetylmuramidases activity (Fig. 1B–D) (Shibata et al., 2005). Different from this branch with *N*-acetylmuramidases domain, all PG-degrading enzymes located in the first branch encode a C-terminal *N*-acetylmuramyl-$_L$-alanine amidase domain, and that one from SS2 strain HA9801 has been identified to function autolytic activity (Ju et al., 2012).

3.3. Identification of AtlA$_{SS}$ as a novel autolysin to be required for truncation of bacterial chain length

Further work constructed the *atlAss* deletion mutant and complemented strains in CZ130302. To avoid the possibility of polar effect, a qRT-PCR analysis was performed that detected the expression of the flanking upstream and downstream genes, ascertaining their transcriptions were not affected (Supplemental Fig. 2). In addition, the growth kinetics of CZ130302 was also not affected by the *atlA*$_{SS}$ deletion (Supplemental Fig. 3).

Homology analysis of the AtlA$_{SS}$ protein revealed that the amino acid sequences shared 33.6% identity with those of the AtlA autolysin protein, which comprised a C-terminal *N*-acetylmuramidases domain in *S. mutans* (Fig. 1C). To verify the putative autolysis activity of AtlA$_{SS}$ in CZ130302, the autolytic assay for CZ130302, Δ*atlA*$_{SS}$ and complemented strains was tested after the pretreatment using Triton X-100, which is a nonionic detergent known to eliminate the inhibition of lipid phosphoric acid on bacterial autolysis system (Neuhaus and Baddiley, 2003). Compared with the *atlA*$_{SS}$ deletion mutant, the CZ130302 and CΔ*atlA*$_{SS}$ strains exhibited an increased autolysis rate (Fig. 2A), suggesting that AtlA$_{SS}$ appears to be a novel autolysin of SS.

To verify the potential correlation between autolytic activity and bacterial chain length, the bacterial cells of WT, Δ*atlA*$_{SS}$ and CΔ*atlA*$_{SS}$ strains were Gram-stained for microscopy. As shown in Fig. 2B, Δ*atlA*$_{SS}$ strain formed significantly longer cell chains, but this change was basically restored by complementation to that of WT strain. Moreover, the addition of purified AtlA$_{SS}$ truncated the long chains of the *atlA*$_{SS}$ deletion mutant into lengths comparable with the WT strain. Further incubation of CZ130302 bacterial cells with anti-AtlA$_{SS}$ antibody resulted in significant extension of chain length to Δ*atlA*$_{SS}$ strain levels, suggesting AtlA$_{SS}$ is responsible for this phenotypic change. The novel autolysin AtlA$_{SS}$ thus plays an important role in modulating bacterial chain length.

3.4. Subcellular localization of AtlA$_{SS}$ in division septum for bacterial separation

The AtlA$_{SS}$ protein possesses a 'GW module' at the N-terminus, which is thought to have a general cell wall-anchoring function (Milohanic et al., 2001). Indirect immunofluorescence analysis detected AtlA$_{SS}$ on the surface of WT strain CZ130302, especially at the division septum location, while fluorescence was not noticed in the Δ*atlA*$_{SS}$ mutant (Fig. 2C). Furthermore, immunogold electron microscopy also confirmed that the labeled AtlA$_{SS}$ concentrated mainly on the septum space (Fig. 2D), which suggests the close relationship between AtlA$_{SS}$ autolysin and bacterial cell division. In fact, it is reasonable to speculate that the subcellular localization of the AtlA$_{SS}$ in the equatorial surface ring somewhat effects cell wall hydrolysis during cell division, which significantly modulates bacterial cell separation, and thus determines chain length.

3.5. AtlA$_{SS}$ is required for the full virulence of SS strain CZ130302

Many studies have reported that autolysins play a key role in the pathogenic process of *Streptococcus* species (Ju et al., 2012; Martner et al., 2008). Hence, we investigated the roles of *atlA*$_{SS}$ gene in SS infection, and scrutinized the LD_{50} evaluation and survivorship curve in the mouse infection model. The LD_{50} values for CZ130302, Δ*atlA*$_{SS}$ and CΔ*atlA*$_{SS}$ were 2.89×10^6, 1.13×10^7, and 3.03×10^6 CFU/mouse, respectively (Fig. 3A). As Fig. 3B shows, we also found that mice groups challenged with the WT and CΔ*atlA*$_{SS}$ strains developed severe clinical signs at 12 h postinfection, and died within almost 5 days; whereas the morbidity and mortality levels in the Δ*atlA*$_{SS}$ challenged group were substantially reduced, with a 40% survival rate. In addition, to better

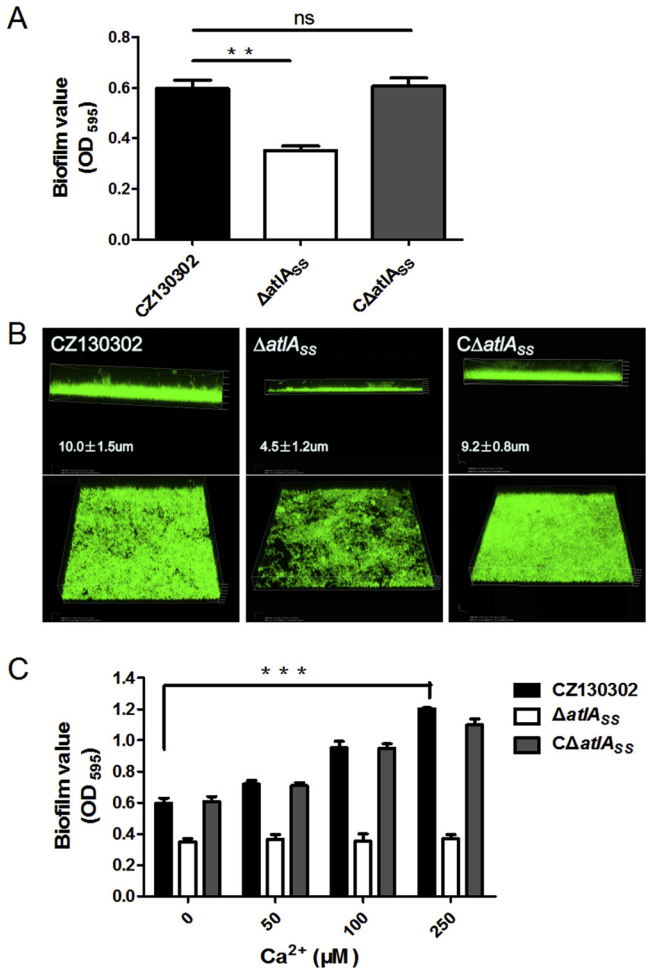

Fig. 4. $AtlA_{SS}$ mediates biofilm formation of SS. (A) Biofilm formation by the WT, Δ*atlA*$_{SS}$ and CΔ*atlA*$_{SS}$. The strains were cultivated in A medium with 1% glucose on 96-well plates, then assayed by crystal violet stain. The OD_{595} of biofilms was measured. Shown are means ± SEM from three independent experiments (** $P < 0.01$). (B) The confocal laser scanning microscopic (CLSM) images of the biofilm formation. The viable bacterial cells presented green fluorescence after the Syto-9 staining. (C) Calcium ions enhance the biofilm formation in SS. Biofilms grown in 96-well plates supplemented with or without calcium ions were stained with crystal violet, then quantified by measuring at OD_{595}. The results are indicated as the means ± SEM from 3 independent experiments (*** $P <$ 0.001) (For interpretation of the references to colour in this figure legend, the reader is referred to the web version of this article).

understand $AtlA_{SS}$ involvement in systemic infection, we also performed the organ-wide bacterial burden assay in infected mice. As shown in Fig. 3C, the bacterial loads in the blood, brains, kidneys and lungs of the mice challenged with Δ*atlA*$_{SS}$ strain were all significantly reduced, versus the WT or CΔ*atlA*$_{SS}$ strains. Taken together, our data suggests that $AtlA_{SS}$ does contribute to CZ130302 virulence.

3.6. *AtlA*$_{SS}$ *mediates biofilm formation in SS*

Bacterial biofilm is thought to be conducive to bacterial resistance of host immune defense and antimicrobial compounds (Jung et al., 2017). The stabilization of bacterial biofilm requires polymers, such as extracellular DNA or glycoproteins, which are the typical products of bacterial lysis (Flemming et al., 2007; Jung et al., 2017). The $AtlA_{SS}$ protein could trigger bacterial cells autolysis, and thus may be involved in SS biofilm formation. To evaluate this potential function of $AtlA_{SS}$, CZ130302 and Δ*atlA*$_{SS}$ strains were cultivated on 96-well polystyrene plates, and then assayed with the crystal violet stain. As expected, the deletion of *atlA*$_{SS}$ caused a significant 40% biofilm reduction, compared to the parental strain CZ130302 ($P <$ 0.01) (Fig. 4A). Besides, biofilms formed by those strains also were stained with Syto-9 fluorescent dye, and visualized through laser scanning confocal microscopy. Three-dimensional images of Δ*atlA*$_{SS}$ strains exhibited poor biofilm formation (Fig. 4B), which is consistent with the results from the crystal violet staining. In *S. mutans,* calcium was the only common human plasma metal ion that enhanced AtlA maturation, increasing biofilm formation (Jung et al., 2017). To test whether this calcium-ion-stimulated $AtlA_{SS}$ maturation was required for biofilm formation in SS strain CZ130302 as well, we evaluated bacterial biofilms grown in 96-well plates supplemented with or without calcium ions. In our research, the enhancing effect of calcium ions was observed in the WT and CΔ*atlA*$_{SS}$ strains, but not in the Δ*atlA*$_{SS}$ strain (Fig. 4C), suggesting the autolytic activity of AtlAss modulated by its maturation was really involved in the SS biofilm formation.

3.7. *The specific interaction between AtlA*$_{SS}$ *and host FG/FN facilitates bacterial adhesion to endothelial cells*

There is no doubt that all functional autolysins are bacterial surface proteins, and our indirect immunofluorescence analysis had already confirmed the cell surface and division septum locations of $AtlA_{SS}$ (Fig. 2C–D). In fact, bacterial surface proteins are often involved in direct interaction with host cells, aiding bacterial colonization and infection (Li et al., 2015; Zhang et al., 2018). The $AtlA_{SS}$ protein was tested for HBMECs binding, with adhesion and indirect immunofluorescence assays. As shown in Fig. 5A, the adherence of the Δ*atlA*$_{SS}$ mutant was significantly reduced in the HBMECs versus the WT or CΔ*atlA*$_{SS}$ strains ($P <$ 0.01). Moreover, obvious green signals were detected in the surface of HBMECs incubated with the recombinant $AtlA_{SS}$ protein, while nothing significant emerged from the negative control (Fig. 5B). These results suggest that the $AtlA_{SS}$ protein may directly interact with some surface factors of host cells.

Host matrix proteins such as FG and FN can serve as the mediators between bacteria and host cells during adhesion (Li et al., 2015). Our study examined the binding of recombinant $AtlA_{SS}$ to the host components. It was observed from these binding assays that the Δ*atlA*$_{SS}$ mutant displayed significantly attenuated binding with FG and FN, versus the WT or complemented strains ($P <$ 0.001) (Fig. 5C). This direct binding between $AtlA_{SS}$ protein and FG or FN was further confirmed by the Far-Western blotting assay. These results suggest that the $AtlA_{SS}$ protein located on the cell surface of the CZ130302 strain could directly interact with FG and FN of host cells (Fig. 5D), and thus may contribute to bacterial adhesion.

4. Discussion

SS is considered to be an important zoonotic pathogen that causes economic and public health problems globally (Goyette-Desjardins et al., 2014; Huang et al., 2019). Raising awareness and understanding of the pathogenesis in SS will help to control and prevent diseases connected to it. Autolytic associated proteins are reportedly involved in many significant physiological activities (Atilano et al., 2014; Jung et al., 2017; Wydau-Dematteis et al., 2018). In the present study, we characterized a novel SS surface protein ($AtlA_{SS}$) with autolytic activity, which contributes to bacterial separation and full virulence in SS infection.

Previous studies have shown that the repetitive GW domains of autolysins were essential for catalytic targeting of the septum location or equatorial surface ring, consequently allowing for localized peptidoglycan hydrolysis (Bublitz et al., 2009; Milohanic et al., 2001). In AtlAss, three tandem repeats comprise the GW domain, suggesting they drive similar functions. Indeed, our results confirm that $AtlA_{SS}$ is mainly located in the cell division septum (Fig. 2C–D). Besides, a conserved *N*-acetylmuramidases domain was also detected in C-terminus of $AtlA_{SS}$,

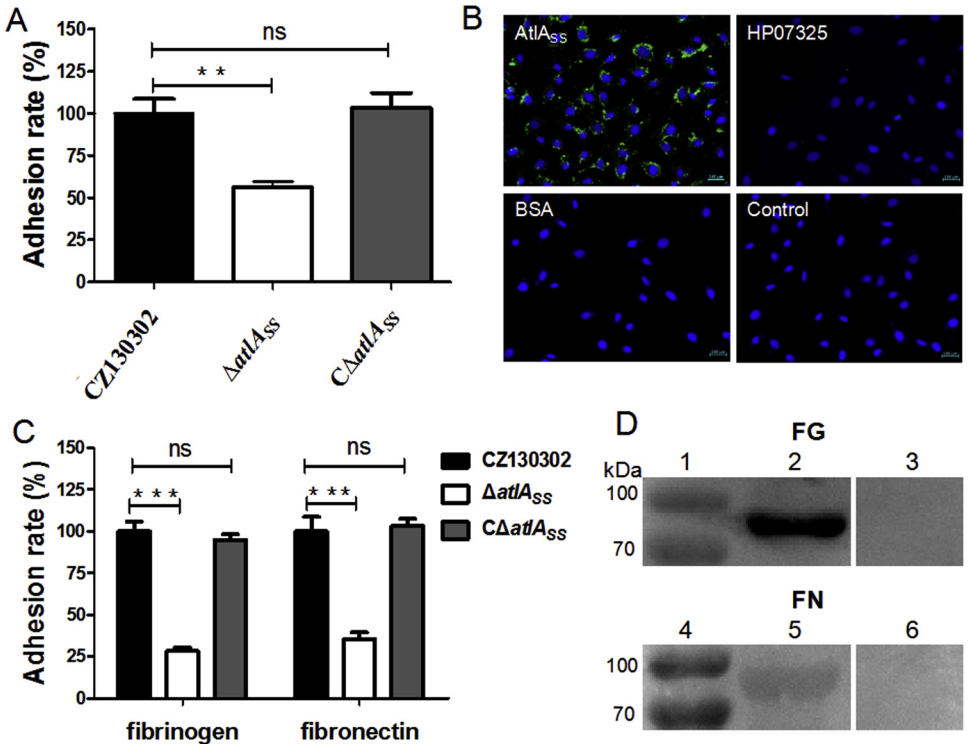

Fig. 5. $AtlA_{SS}$ promotes adherence to host cells and interacts specifically with host proteins FG and FN. (A) Contribution of $AtlA_{SS}$ to the adhesion to HBMEC cells. The adhesion rate of WT group was designed as 100% arbitrarily. The data showed means with standard deviations for the results from three independent experiments carried out in triplicate. Two-tailed unpaired *t* tests were used for statistical analysis (** $P < 0.01$). (B) Adherence of $AtlA_{SS}$ to HBMEC cells detected by the immunofluorescence assay. HBMEC cells were incubated with recombinant protein $AtlA_{SS}$, while the samples without the His tag monoclonal antibody were set as the blank control. The intracellular nucleoid was stained with DAPI in blue and the $AtlA_{SS}$ protein was detected with FITC conjugated the goat anti-mouse IgG (H + L) in green. Green bars represent 100 μm. (C) Binding of CZ130302, Δ*atlA*$_{SS}$ and CΔ*atlA*$_{SS}$ to the fibrinogen and fibronectin. The 12-well plates were coated with FG or FN, then incubated with the SS strains. The number of bacteria on each plate was measured. Shown are means ± SEM from three independent experiments (*** $P < 0.001$). (D) Assessment of the binding of $AtlA_{SS}$ to fibrinogen and fibronectin by Far-western blotting. Recombinant protein $AtlA_{SS}$ was separated by the SDS-PAGE and then transferred onto PVDF membranes. The membranes were incubated with human FG or FN, then detected by primary antibodies and corresponding secondary antibodies. Un-incubated FG/FN membranes were performed as negative control (line3; line6) (For interpretation of the references to colour in this figure legend, the reader is referred to the web version of this article).

which is generally considered as a catalytically active domain that hydrolyzes the peptidoglycan cell wall (Shibata et al., 2005; Stojkovic and Rothman-Denes, 2007). These observations strongly urge us to further verify that $AtlA_{SS}$ really could mediate the peptidoglycan hydrolysis in the primary septum of cell division and separation (Fig. 2B). However, the aimless or excessive hydrolysis of peptidoglycan, induced by specific conditions, can cause bacterial suicide, as seen with the Triton X-100 induced autolysis in the CZ130302 strain. Thus, fine-tuning the activity of PGH is essential to the survival of bacteria (Jung et al., 2017; Vollmer et al., 2008). In *Streptococcus mutans*, the VicK sensor was found to be responsible for calcium ion sensing, and induction of AtlA maturation (Jung et al., 2017). ComE and CiaR also have been demonstrated to be involved in the expression of the LytA activity on the pneumococcal surface (Pinas et al., 2008). In addition, the secondary cell wall polymers, such as polysaccharides and teichoic acids, were also proven to modulate autolytic activity by shielding peptidoglycan (Hanson and Neely, 2012). However, the underlying regulation of AtlAss function is relatively unknown, and should be further explored.

It is well known that the deficiency of cell separation will cause a significantly long chain length in *Streptococcus*, which visibly benefits the bacterial adhesion to host cells (Rodriguez et al., 2012; Tan et al., 2017). However, the *atlAss* deletion mutant, with a longer chain, showed a significant decrease in cell adhesion, hinting at possible $AtlA_{SS}$ activity during this process. Indeed, $AtlA_{SS}$ is exposed on the bacterial surface (Fig. 2C), a condition essential to its host cell adhesion functionality. Asano et al. verified that the autolysin Ami can exploit interaction of repetitive GW domains with glycosaminoglycans, thus promoting the adhesion of *L. monocytogenes* to mouse hepatocytes (Asano et al., 2012). Autolysin Aas of *Staphylococcus saprophyticus* has a strong fibronectin-binding activity (Mortimer et al., 2017), while AtlE of *Staphylococcus epidermidis* could bind vitronectin (Heilmann et al., 1997). Our study also establishes the role of $AtlA_{SS}$ in SS adhesion, which is consistent with the above research, thus confirming that $AtlA_{SS}$ facilitates adhesive fibrinogen/fibronectin-binding activity (Fig. 5C–D). Similarly, Milohanic et al. proposed that the repetitive GW domains among the various autolysin molecules are not conserved, thus accepting different cell surface receptors (Milohanic et al., 2001), which may enable bacterial pathogens to colonize particular ecological niches.

Compared with the wild-type strain, *atlA*$_{SS}$ mutant displayed a weaker virulence (Fig. 3). The role of $AtlA_{SS}$ in biofilm formation and host cell adhesion is probably an important element during infection. The continuous remodeling of cell wall in Gram-positive bacteria is also important for the release and presence of factors reported to affect bacterial virulence (Bublitz et al., 2009; Johnson et al., 2013). In *Clostridium difficile*, the novel peptidoglycan hydrolase Cwp19 is required for the release of clostridial glucosylating toxins (TcdA and TcdB), to contribute to bacterial virulence (Wydau-Dematteis et al., 2018). Moreover, the major autolysin LytA of *S. pneumonia* could cause dramatic autolysis, resulting in pneumolysin release, which is toxic to a series of host cells, and also modulates inflammatory reaction (Martner et al., 2008). Hence, it is worth investigating whether the autolysin $AtlA_{SS}$ mediates the release of intracellular components, or suilysin, which contribute to SS virulence.

To summarize this, we screened a putative SS autolysin, $AtlA_{SS}$, through genomic retrieval and sequence alignment. $AtlA_{SS}$ was confirmed to be involved in the daughter cell division, bacterial chain length, autolysis, cell adhesion, biofilm formation and pathogenicity. These results will provide interesting insights into SS pathogenesis.

Acknowledgments

This work was supported by the Development Program of Jiangsu Modern Agricultural Industry Technology System (No. JSTS[2018] 011), Postgraduate Research & Practice Innovation Program of Jiangsu Province (No. KYCX18_0717), Shanghai Agriculture Applied Technology Development Program (No. G2016060201), the Special Fund for Public Welfare Industry of Chinese Ministry of Agriculture

(No. 201303041) and the project funded by the Priority Academic Program Development of Jiangsu Higher Education Institutions (PAPD).

Appendix A. Supplementary data

Supplementary material related to this article can be found, in the online version, at doi:https://doi.org/10.1016/j.vetmic.2019.05.020.

References

Asano, K., Kakizaki, I., Nakane, A., 2012. Interaction of Listeria monocytogenes autolysin amidase with glycosaminoglycans promotes listerial adhesion to mouse hepatocytes. Biochimie 94, 1291–1299.

Atilano, M.L., Pereira, P.M., Vaz, F., Catalao, M.J., Reed, P., Grilo, I.R., Sobral, R.G., Ligoxygakis, P., Pinho, M.G., Filipe, S.R., 2014. Bacterial autolysins trim cell surface peptidoglycan to prevent detection by the Drosophila innate immune system. eLife 3, e02277.

Bonnet, J., Durmort, C., Jacq, M., Mortier-Barriere, I., Campo, N., VanNieuwenhze, M.S., Brun, Y.V., Arthaud, C., Gallet, B., Moriscot, C., Morlot, C., Vernet, T., Di Guilmi, A.M., 2017. Peptidoglycan O-acetylation is functionally related to cell wall biosynthesis and cell division in Streptococcus pneumoniae. Mol. Microbiol. 106, 832–846.

Bublitz, M., Polle, L., Holland, C., Heinz, D.W., Nimtz, M., Schubert, W.D., 2009. Structural basis for autoinhibition and activation of Auto, a virulence-associated peptidoglycan hydrolase of Listeria monocytogenes. Mol. Microbiol. 71, 1509–1522.

Flemming, H.C., Neu, T.R., Wozniak, D.J., 2007. The EPS matrix: the "house of biofilm cells". J. Bacteriol. 189, 7945–7947.

Goyette-Desjardins, G., Auger, J.P., Xu, J., Segura, M., Gottschalk, M., 2014. Streptococcus suis, an important pig pathogen and emerging zoonotic agent-an update on the worldwide distribution based on serotyping and sequence typing. Emerg. Microbes Infect. 3, e45.

Hanson, B.R., Neely, M.N., 2012. Coordinate regulation of Gram-positive cell surface components. Curr. Opin. Microbiol. 15, 204–210.

Heilmann, C., Hussain, M., Peters, G., Gotz, F., 1997. Evidence for autolysin-mediated primary attachment of Staphylococcus epidermidis to a polystyrene surface. Mol. Microbiol. 24, 1013–1024.

Huang, J., Liu, X., Chen, H., Chen, L., Gao, X., Pan, Z., Wang, J., Lu, C., Yao, H., Wang, L., Wu, Z., 2019. Identification of six novel capsular polysaccharide loci (NCL) from Streptococcus suis multidrug resistant non-typeable strains and the pathogenic characteristic of strains carrying new NCLs. Transbound. Emerg. Dis.

Johnson, J.W., Fisher, J.F., Mobashery, S., 2013. Bacterial cell-wall recycling. Ann. N. Y. Acad. Sci. 1277, 54–75.

Ju, C.X., Gu, H.W., Lu, C.P., 2012. Characterization and functional analysis of atl, a novel gene encoding autolysin in Streptococcus suis. J. Bacteriol. 194, 1464–1473.

Jung, C.J., Hsu, R.B., Shun, C.T., Hsu, C.C., Chia, J.S., 2017. AtlA mediates extracellular DNA release, which contributes to Streptococcus mutans biofilm formation in an experimental rat model of infective endocarditis. Infect. Immun. 85.

Layec, S., Decaris, B., Leblond-Bourget, N., 2008. Diversity of Firmicutes peptidoglycan hydrolases and specificities of those involved in daughter cell separation. Res. Microbiol. 159, 507–515.

Li, Q., Fu, Y., He, Y., Zhang, Y., Qian, Y., Yu, Y., Yao, H., Lu, C., Zhang, W., 2017. Fibronectin-/fibrinogen-binding protein (FBPS) is not a critical virulence factor for the Streptococcus suis serotype 2 strain ZY05719. Vet. Microbiol. 208, 38–46.

Li, Q., Liu, H., Du, D., Yu, Y., Ma, C., Jiao, F., Yao, H., Lu, C., Zhang, W., 2015. Identification of novel laminin- and fibronectin-binding proteins by far-western blot: capturing the adhesins of Streptococcus suis type 2. Front. Cell. Infect. Microbiol. 5, 82.

Martner, A., Dahlgren, C., Paton, J.C., Wold, A.E., 2008. Pneumolysin released during Streptococcus pneumoniae autolysis is a potent activator of intracellular oxygen radical production in neutrophils. Infect. Immun. 76, 4079–4087.

Mehta, K.K., Paskaleva, E.E., Azizi-Ghannad, S., Ley, D.J., Page, M.A., Dordick, J.S., Kane, R.S., 2013. Characterization of AmiBA2446, a novel bacteriolytic enzyme active against Bacillus species. Appl. Environ. Microbiol. 79, 5899–5906.

Milohanic, E., Jonquieres, R., Cossart, P., Berche, P., Gaillard, J.L., 2001. The autolysin Ami contributes to the adhesion of Listeria monocytogenes to eukaryotic cells via its cell wall anchor. Mol. Microbiol. 39, 1212–1224.

Mortimer, T.D., Annis, D.S., O'Neill, M.B., Bohr, L.L., Smith, T.M., Poinar, H.N., Mosher, D.F., Pepperell, C.S., 2017. Adaptation in a fibronectin binding autolysin of Staphylococcus saprophyticus. mSphere 2.

Neuhaus, F.C., Baddiley, J., 2003. A continuum of anionic charge: structures and functions of D-alanyl-teichoic acids in gram-positive bacteria. Microbiol. Mol. Biol. Rev. 67, 686–723.

Pan, Z., Ma, J., Dong, W., Song, W., Wang, K., Lu, C., Yao, H., 2015. Novel variant serotype of streptococcus suis isolated from piglets with meningitis. Appl. Environ. Microbiol. 81, 976–985.

Pilgrim, S., Kolb-Maurer, A., Gentschev, I., Goebel, W., Kuhn, M., 2003. Deletion of the gene encoding p60 in Listeria monocytogenes leads to abnormal cell division and loss of actin-based motility. Infect. Immun. 71, 3473–3484.

Pinas, G.E., Cortes, P.R., Orio, A.G., Echenique, J., 2008. Acidic stress induces autolysis by a CSP-independent ComE pathway in Streptococcus pneumoniae. Microbiology 154, 1300–1308.

Rodriguez-Cerrato, V., Garcia, P., Huelves, L., Garcia, E., Del Prado, G., Gracia, M., Ponte, C., Lopez, R., Soriano, F., 2007. Pneumococcal LytA autolysin, a potent therapeutic agent in experimental peritonitis-sepsis caused by highly beta-lactam-resistant Streptococcus pneumoniae. Antimicrob. Agents Chemother. 51, 3371–3373.

Rodriguez, J.L., Dalia, A.B., Weiser, J.N., 2012. Increased chain length promotes pneumococcal adherence and colonization. Infect. Immun. 80, 3454–3459.

Scheffers, D.J., Pinho, M.G., 2005. Bacterial cell wall synthesis: new insights from localization studies. Microbiol. Mol. Biol. Rev. 69, 585–607.

Shibata, Y., Kawada, M., Nakano, Y., Toyoshima, K., Yamashita, Y., 2005. Identification and characterization of an autolysin-encoding gene of Streptococcus mutans. Infect. Immun. 73, 3512–3520.

Stinemetz, E.K., Gao, P., Pinkston, K.L., Montealegre, M.C., Murray, B.E., Harvey, B.R., 2017. Processing of the major autolysin of E. faecalis, AtlA, by the zinc-metalloprotease, GelE, impacts AtlA septal localization and cell separation. PLoS One 12, e0186706.

Stojkovic, E.A., Rothman-Denes, L.B., 2007. Coliphage N4 N-acetylmuramidase defines a new family of murein hydrolases. J. Mol. Biol. 366, 406–419.

Tan, M.F., Liu, W.Q., Zhang, C.Y., Gao, T., Zheng, L.L., Qiu, D.X., Li, L., Zhou, R., 2017. The involvement of MsmK in pathogenesis of the Streptococcus suis serotype 2. MicrobiologyOpen 6.

Tang, J., Wang, C., Feng, Y., Yang, W., Song, H., Chen, Z., Yu, H., Pan, X., Zhou, X., Wang, H., Wu, B., Wang, H., Zhao, H., Lin, Y., Yue, J., Wu, Z., He, X., Gao, F., Khan, A.H., Wang, J., Zhao, G.P., Wang, Y., Wang, X., Chen, Z., Gao, G.F., 2006. Streptococcal toxic shock syndrome caused by Streptococcus suis serotype 2. PLoS Med. 3, e151.

Vollmer, W., Blanot, D., de Pedro, M.A., 2008. Peptidoglycan structure and architecture. FEMS Microbiol. Rev. 32, 149–167.

Wydau-Dematteis, S., El Meouche, I., Courtin, P., Hamiot, A., Lai-Kuen, R., Saubamea, B., Fenaille, F., Butel, M.J., Pons, J.L., Dupuy, B., Chapot-Chartier, M.P., Peltier, J., 2018. Cwp19 is a novel lytic transglycosylase involved in stationary-phase autolysis resulting in toxin release in Clostridium difficile. mBio 9.

Zhang, Y., Lu, P., Pan, Z., Zhu, Y., Ma, J., Zhong, X., Dong, W., Lu, C., Yao, H., 2018. Sssp1, a Streptococcus suis fimbriae-like protein transported by SecY2/A2 system contributes to bacterial virulence. Appl. Environ. Microbiol.

Zhu, Y., Dong, W., Ma, J., Zhang, Y., Pan, Z., Yao, H., 2019. Utilization of the ComRS system for the rapid markerless deletion of chromosomal genes in Streptococcus suis. Future Microbiol.